DEM Error Correction in InSAR Time Series

Heresh Fattahi, *Student Member, IEEE*, and Falk Amelung

***Abstract*—We present a mathematical formulation for the phase due to the errors in digital elevation models (DEMs) in synthetic aperture radar (SAR) interferometry (InSAR) time series obtained by the small baseline (SB) or the small baseline subset method. We show that the effect of the DEM error in the estimated displacement is proportional to the perpendicular baseline history of the set of SAR acquisitions. This effect at a given epoch is proportional to the perpendicular baseline between the SAR acquisition at that epoch and the reference acquisition. Therefore, the DEM error can significantly affect the time-series results even if SB interferograms are used. We propose a new method for DEM error correction of InSAR time series, which operates in the time domain after inversion of the network of interferograms for the displacement time series. This is in contrast to the method of Berardino *et al.* (2002) in which the DEM error is estimated in the interferogram domain. We show the effectiveness of this method using simulated InSAR data. We apply the new method to Fernandina volcano in the Galapagos Islands and show that the proposed DEM error correction improves the estimated displacement significantly.**

***Index Terms*—Baseline history, digital elevation model (DEM) error, synthetic aperture radar (SAR) interferometry (InSAR), time series.**

I. Introduction

DIFFERENTIAL synthetic aperture radar (SAR) interferometry (InSAR) is a powerful technique to estimate the land surface deformation caused by natural and anthropogenic processes including earthquakes, volcanic eruptions, landslides, and hydrological subsidence[1]–[4]. The temporal evolution of surface deformation can be reconstructed from a set of SAR acquisitions using InSAR-time-series techniques, such as small baseline (SB) [5]–[8] or persistent scatterer (PS) [9]–[12]. In the SB technique, the phase history with respect to the first acquisition is reconstructed from a network of interferograms with small spatial and temporal baselines, which ensures maximum interferometric coherence. Small baseline subset (SBAS) is a well-known SB technique in which the independent subsets of interferograms are combined to estimate the displacement history using the minimum-length solution of the phase velocity obtained by singular-value decomposition [5].

Estimation of ground displacement using InSAR requires the removal of phase contributions due to the Earth's topography from the interferograms. The topography is approximated using a digital elevation model (DEM), and then, the topographic phase is estimated using information about the imaging geometry. In practice, this is usually accomplished along with removing the phase due to the earth curvature in a processing step commonly referred to as flattening [13], carried out before interferogram filtering [14]. The topographic phase is proportional to the perpendicular baseline separation between the two SAR images forming the interferogram. Errors in the DEM lead to baseline-dependent phase residuals in the interferograms, which, if not removed, leads to errors in the displacement history [5].

Here, we present a mathematical formulation for the phase due to the DEM error in the InSAR time domain. We show that the phase due to the DEM error at each epoch is proportional to the perpendicular baseline between the SAR acquisition at that epoch and the reference acquisition (and not to the perpendicular baseline of individual interferograms). This explains the unexpectedly large effects of DEM errors in SBAS results noted in [5] and why the DEM error correction is necessary despite the use of SB interferograms. Thus, the use of SB interferograms does not necessarily minimize the effect of DEM error. We propose a new method to correct for DEM errors in the time domain, which is, under certain conditions, equivalent to the method in [5] in the interferogram. Original SBAS uses interferometric phases to estimate the DEM error and then inverts the corrected interferograms to estimate the phase velocities [5]. An alternative has been presented to estimate the DEM error in the advanced land observing satellite (ALOS) phased array type L-band SAR (PALSAR) data by inverting interferometric phases to jointly estimate the DEM error and phase velocities [15]. Here, we present a new algorithm to estimate the DEM error after the time-series inversion of interferometric phases. Our proposed method for DEM error correction in the time domain is different from the method in [16] in that we estimate the parameters of low-pass displacement instead of applying low-pass filtering. Also, our method uses the phase velocity history instead of the phase history, which can have significant effect on DEM error estimation in the case of time-variable displacement.

There are several potential advantages of the DEM error correction in the time domain compared to that in the interferogram domain. First, it is more efficient because design matrices are smaller. Second, the employment of alternative temporal deformation models is straightforward (such as the offset due to an earthquake). Third, it facilitates the identification and correction of orbital errors as well as atmospheric contributions, which are most efficiently applied in the time domain [9], [17]. Finally, it is independent of the network of interferograms. As we will show in the following, in the interferogram domain, the network may affect the DEM error estimation if the displacements are not well approximated by the assumed deformation model.

This paper is organized as follows. Section II presents the mathematical formulation of the phase due to the DEM error

Manuscript received March 9, 2012; revised June 6, 2012 and September 4, 2012; accepted October 24, 2012. Date of publication January 29, 2013; date of current version June 20, 2013. This work was supported in part by the National Science Foundation under Grant EAR 1019847 and in part by the National Aeronautics and Space Administration under Grant NNX09AK72G.

The authors are with the Division of Marine Geology and Geophysics, Rosenstiel School of Marine and Atmospheric Science, University of Miami, Miami, FL 33149-1098 USA (e-mail: hfattahi@rsmas.miami.edu; famelung@rsmas.miami.edu).

Digital Object Identifier 10.1109/TGRS.2012.2227761

in InSAR time series. A new algorithm for the DEM error correction is proposed in Section III. The experimental results of the proposed algorithm using simulated and real data sets are discussed in Sections IV and V, and the conclusion is presented in Section VI.

II. Phase due to the DEM Error in the InSAR Time Series

Let us start with the differential interferometric phase corrected for earth curvature and topographic effects. By considering an interferogram formed from two SAR acquisitions at times t_A and t_B, we can write the following formula for each pixel [5], [16]:

$$\begin{aligned}\Delta\phi(t_A,t_B) = &\Delta\phi_{\rm def}(t_A,t_B) + \Delta\phi^{\varepsilon}_{\rm topo}(t_A,t_B)\\ &+ \Delta\phi_{\rm atm}(t_A,t_B) + \Delta\phi^{\varepsilon}_{\rm orb}(t_A,t_B)\\ &+ \Delta\phi_{\rm noise}(t_A,t_B)\end{aligned} \tag{1}$$

where $\Delta\phi(t_A,t_B)$ represents the measured interferometric phase, $\Delta\phi_{\rm def}(t_A,t_B)$ represents the phase due to the ground displacement in the radar line-of-sight direction between times t_A and t_B, $\Delta\phi^{\varepsilon}_{\rm topo}(t_A,t_B)$ represents the interferometric phase due to the error in the DEM used for topographic phase estimation, $\Delta\phi_{\rm atm}(t_A,t_B)$ represents the phase due to the differences in atmospheric delay between t_A and t_B, $\Delta\phi^{\varepsilon}_{\rm orb}(t_A,t_B)$ represents the phase due to the orbital error, and $\Delta\phi_{\rm noise}(t_A,t_B)$ represents the phase due to different decorrelation phenomena and thermal noise. The accuracy of the DEM, as an estimation of the Earth's topography, is limited by the method and instruments used for generating the DEM. Also, the topography of the Earth may change with time. The height of the Earth's topography ($z_{\rm topo}$) is approximated by a DEM such that $z_{\rm topo} = z_{\rm DEM} + z^{\varepsilon}$, with $z_{\rm DEM}$ being the height of the DEM and z^{ε} being the error of the DEM. After the topographic phase estimation, the phase due to the DEM error remains in the differential interferograms and can be expressed for each pixel as [1]

$$\Delta\phi^{\varepsilon}_{\rm topo}(t_A,t_B) = \frac{4\pi}{\lambda}\frac{B_{\perp}(t_A,t_B)}{r\sin(\theta)}z^{\varepsilon} \tag{2}$$

where $B_{\perp}(t_A,t_B)$ is the perpendicular baseline between the two SAR acquisitions, r is the range between the target and the SAR antenna, θ is the look angle, and λ is the transmitted signal central wavelength.

InSAR is a relative measurement technique measuring displacement at the time of the slave image since the master acquisition. Accordingly, InSAR time series resolve displacement relative to a reference time. In the SBAS method, the first acquisition is commonly used as the reference acquisition. We substitute $B_{\perp}(t_A,t_B)$ in (2) by the difference of perpendicular baselines between the SAR images acquired at times t_B and t_A and the reference acquisition, i.e., $B_{\perp}(t_A,t_B) = B_{\perp}(t_B) - B_{\perp}(t_A)$ (see Appendix A), and rewrite (1)

$$\begin{aligned}\Delta\phi(t_A,t_B) = &\frac{4\pi}{\lambda}\left(d(t_B) - d(t_A)\right)\\ &+ \frac{4\pi}{\lambda}\left(\frac{B_{\perp}(t_B) - B_{\perp}(t_A)}{r\sin(\theta)}\right)z^{\varepsilon}\\ &+ \phi_{\rm atm}(t_B) - \phi_{\rm atm}(t_A) + \Delta\phi^{\varepsilon}_{\rm orb}(t_A,t_B)\\ &+ \Delta\phi_{\rm noise}(t_A,t_B)\end{aligned} \tag{3}$$

where $B_{\perp}(t_B)$ is the perpendicular baseline between the SAR acquisition at t_B and the reference acquisition. Similarly, $B_{\perp}(t_A)$ is the perpendicular baseline between the acquisition at t_A and the reference acquisition. $d(t_A)$ and $d(t_B)$ are the line-of-sight displacements at t_A and t_B with respect to the reference acquisition, respectively. $\phi_{\rm atm}(t_A)$ and $\phi_{\rm atm}(t_B)$ are the phases due to the atmospheric delay at times t_A and t_B, respectively.

In the SBAS algorithm, a set of phase-unwrapped interferograms formed from $N+1$ SAR acquisitions is inverted to reconstruct the phase history $\phi(t_i)$ at N epochs $(t_1,\ldots,t_N)$ with respect to the reference acquisition at t_0, implying that $\phi(t_0) = 0$

$$\phi(t_i) = \frac{4\pi}{\lambda}d(t_i) + \phi^{\varepsilon}_{\rm topo}(t_i) + \phi^{\varepsilon}_{\rm orb}(t_i) + \phi_{\rm atm}(t_i) + \phi_{\rm noise}(t_i) \tag{4}$$

wherein $d(t_i)$ is the cumulative line-of-sight displacement at time t_i and $\phi^{\varepsilon}_{\rm topo}(t_i)$, $\phi_{\rm atm}(t_i)$, $\phi^{\varepsilon}_{\rm orb}(t_i)$, and $\phi_{\rm noise}(t_i)$ are the phase histories due to the DEM error, atmospheric delay, orbital error, and noise, respectively, with respect to the reference acquisition. By considering (3), the phase due to the DEM error can be expressed as

$$\phi^{\varepsilon}_{\rm topo}(t_i) = \frac{4\pi}{\lambda}\frac{B_{\perp}(t_i)}{r\sin(\theta)}z^{\varepsilon} \tag{5}$$

where $B_{\perp}(t_i)$ represents the baseline history of SAR acquisitions. $B_{\perp}(t_i)$ at each time epoch t_i is the perpendicular baseline between the SAR image acquired at that time and the reference acquisition (see Appendix A). According to (5), it is clear that the phase history due to the DEM error is proportional to the baseline history. This means that, while selecting small-spatial-baseline interferograms in the SBAS method minimizes the phase due to the DEM error in individual interferograms, it does not reduce this effect in the estimated phase history. The phase due to the DEM error in the estimated phase history is minimized only when a set of SAR acquisitions with a small range of perpendicular baselines exists. This is why the SBAS technique requires a DEM error correction even though SB interferograms are used.

III. Proposed Method for the DEM Error Correction

By considering (4), the estimated phase history includes the displacement and the effects of DEM error, atmospheric delay, remaining orbital errors, and noise. To estimate the DEM error (z^{ε}), by following that in [5], we consider a cubic temporal deformation model as follows:

$$\phi_{\rm def}(t_i) = \bar{v}(t_i - t_0) + \frac{1}{2}\Delta\bar{a}(t_i - t_0)^2 + \frac{1}{6}\Delta\bar{a}(t_i - t_0)^3 \tag{6}$$

where $\bar{v}$ is the mean velocity, $\bar{a}$ is the mean acceleration, and $\Delta\bar{a}$ is the mean acceleration variation. Also, other assumptions, including simpler models or more complicated models considering specific events like earthquakes or volcanic eruptions, could be used in (6). Accordingly, the design matrix which

follows (9) also changes. By substituting (5) and (6) into (4), we obtain

$$\phi(t_i) =, \bar{v}(t_i - t_0) + \frac{1}{2}\bar{a}(t_i - t_0)^2 + \frac{1}{6}\Delta\bar{a}(t_i - t_0)^3 + \frac{4\pi}{\lambda}\frac{B_\perp(t_i)}{r\sin(\theta)}z^\varepsilon + \psi(t_i) \quad (7)$$

wherein $\psi(t_i)$ represents different high-frequency components including the phase due to the atmospheric delay, remaining effects of orbital error, noise, and high-frequency components of the displacement which was not considered in the deformation model. By following the original SBAS method, we now rewrite (7) in terms of the phase velocity history between two consecutive epochs $v_i = (\phi(t_i) - \phi(t_{i-1}))/(t_i - t_{i-1})$, with $i = 1, \ldots, N$ (see Appendix B)

$$v_i = \bar{v} + \frac{1}{2}\bar{a}(t_i + t_{i-1} - 2t_0) + \frac{(t_i - t_0)^3 - (t_{i-1} - t_0)^3}{6(t_i - t_{i-1})}\Delta\bar{a} + \frac{4\pi}{\lambda}\frac{\dot{B}_{\perp i}}{r\sin(\theta)}z^\varepsilon + \dot{\psi}_i \quad (8)$$

where $\dot{B}_{\perp i}$ is the baseline velocity history defined as $\dot{B}_{\perp i} = (B_\perp(t_i) - B_\perp(t_{i-1}))/(t_i - t_{i-1})$, with $i = 1, \ldots, N$, and $\dot{\psi}_i$ is the temporal gradient of $\psi(t_i)$, considered as noise in the DEM error estimation process. To estimate the DEM error and the parameters of the assumed deformation model, a linear system with N equations is formed for each pixel as follows:

$$V = AX + n \quad (9)$$

wherein $V^{\mathrm{T}} = [v_1, v_2, \ldots, v_N]$ is a vector of estimated phase velocities obtained from the inversion of uncorrected interferometric phases using regular SBAS, $X^{\mathrm{T}} = [\bar{v}, \bar{a}, \Delta\bar{a}, z^\varepsilon]$ is the vector of unknown parameters, n is the residual vector, and A is an $(N \times 4)$ design matrix

$$A = \begin{bmatrix} 1 & \frac{(t_1 - t_0)}{2} & \frac{1}{6}(t_1 - t_0)^2 & \frac{4\pi}{\lambda}\frac{\dot{B}_{\perp 1}}{r\sin(\theta)} \\ 1 & \frac{(t_2 + t_1 - 2t_0)}{2} & \frac{(t_2 - t_0)^3 - (t_1 - t_0)^3}{6(t_2 - t_1)} & \frac{4\pi}{\lambda}\frac{\dot{B}_{\perp 2}}{r\sin(\theta)} \\ \vdots & \vdots & \vdots & \vdots \\ 1 & \frac{(t_N + t_{N-1} - 2t_0)}{2} & \frac{(t_N - t_0)^3 - (t_{N-1} - t_0)^3}{6(t_N - t_{N-1})} & \frac{4\pi}{\lambda}\frac{\dot{B}_{\perp N}}{r\sin(\theta)} \end{bmatrix}. \quad (10)$$

The solution of this linear system of equations generally can be obtained by minimizing the L_p norm of residuals, which can be written as follows:

$$\hat{X} = \arg\min \|n\|_p = \arg\min \|V - AX\|_p = \arg\min \left(\sum_{i=1}^{N} |V - AX|_i^p\right)^{\frac{1}{p}}, \qquad p \geq 1 \quad (11)$$

where $\hat{X}$ is the estimated vector of unknown parameters and p is the power. In this paper, we use L_2-*norm* minimization (unweighted least squares) to obtain the solution

$$\hat{X} = (A^{\mathrm{T}}A)^{-1}A^{\mathrm{T}}V. \quad (12)$$

After the estimation of z^ε, the contribution to the phase is calculated using (5) and removed from $\phi(t_i)$. The estimated phase history after DEM error correction may still be affected by the other sources of error like atmospheric delay. Thus, the next step is to remove the atmospheric delays, which is beyond the scope of this paper. Usually, spatial–temporal filtering is used for this purpose [5], [9].

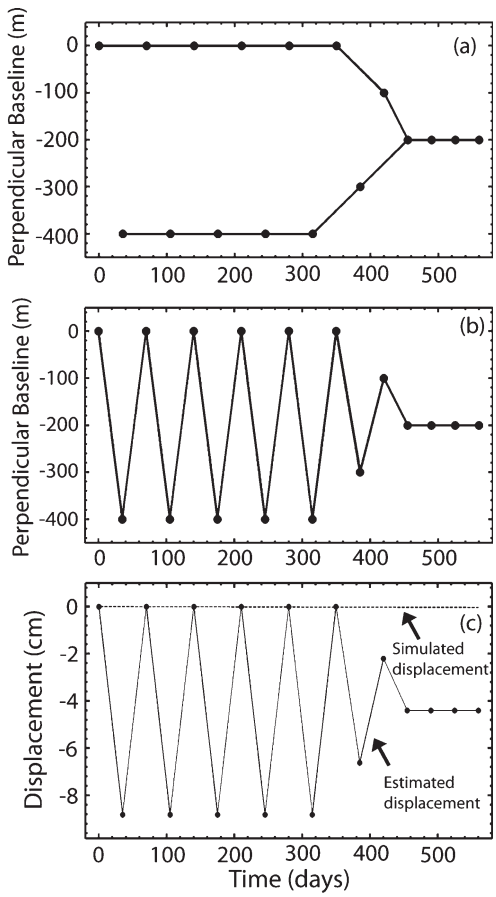

Fig. 1. Simulated data illustrating the effect of the DEM error in InSAR time series. (a) Baseline–time plot of the network of interferograms. (b) Perpendicular baseline history. (c) (Dashed line) Simulated displacement history and (solid line) estimated displacement history without DEM error correction. The estimated displacement is affected by the DEM error and proportional to the baseline history.

IV. Simulated Data

We demonstrate the effect of DEM errors in InSAR time series using simulations. We specify a displacement history, the time and perpendicular baseline of a set of interferograms (i.e., the baseline history), and a DEM error. We then generate a set of simulated interferograms and invert it for the displacement history without DEM error correction and using different DEM error correction methods. We assess the quality of the DEM error correction method by comparison of the estimated with the original simulated displacement history.

A. Illustration of the DEM Error

To illustrate the DEM error in InSAR time series, we assume no ground deformation (zero displacement), a DEM error of 50 m, and the network of interferograms as shown in Fig. 1(a). The network consists of two branches of zero-baseline interferograms, which connect to one single branch for the last few

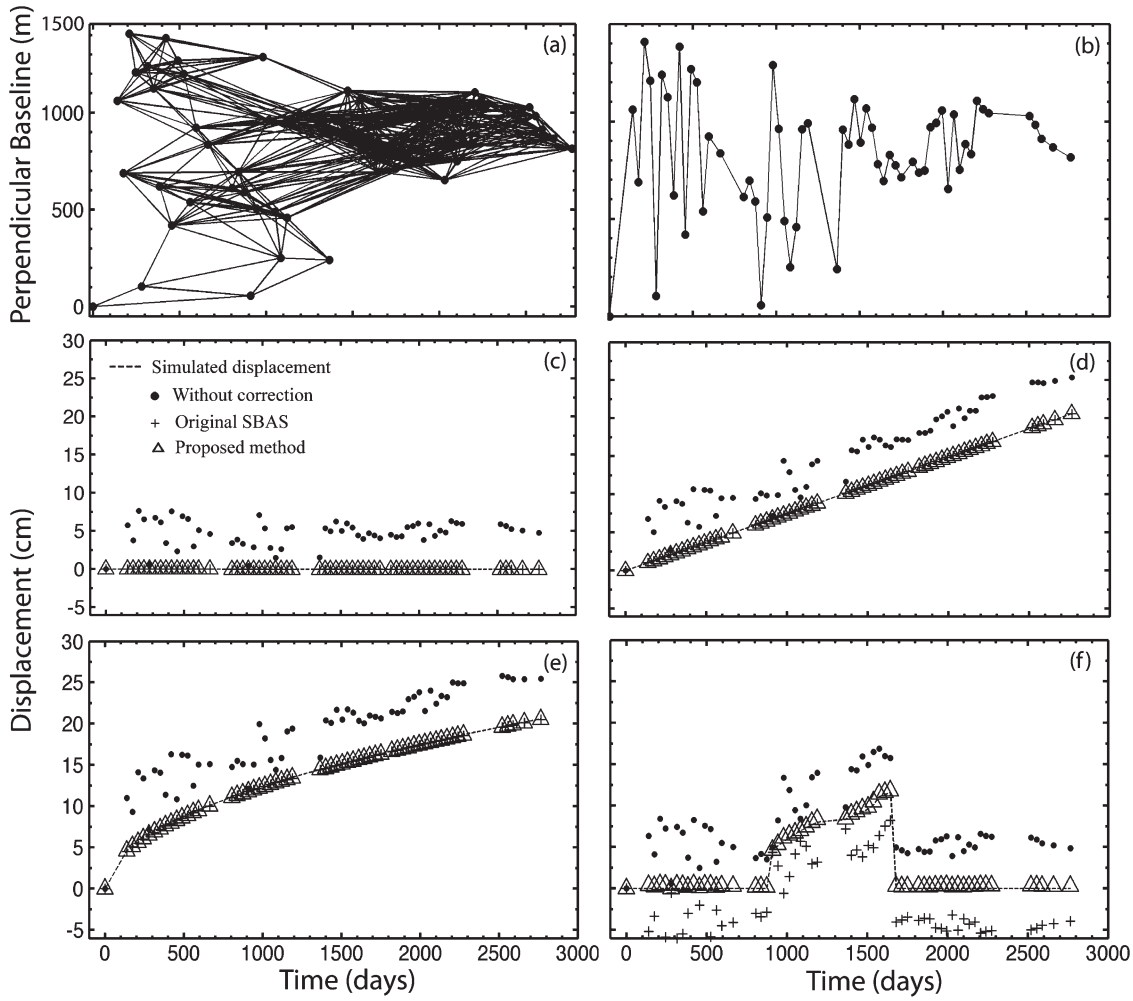

Fig. 2. Application of the new DEM error correction algorithm on the simulated data considering different temporal variations of ground displacement: (a) Baseline-time plot of the network of interferograms and (b) baseline history. (c)–(f) (Dashed lines) Simulated displacement history and the estimated displacement histories (filled circles) without DEM error correction, (triangles) DEM error corrected using the new algorithm, and (plus signs) DEM error corrected using the original SBAS method for a pixel with (c) zero, (d) linear, (e) exponential, and (f) complex time-variable displacements. The baseline history is taken from real Envisat SAR data acquired over Fernandina volcano (see Section V). Note that the proposed and the original SBAS method achieve identical results for the cases presented in (c)–(e).

acquisitions. The 16 interferograms of the network have small perpendicular baselines (< 200 m) with 12 of them with zero baseline. The baseline history varies by 400 m between the first 13 acquisitions and is constant for the last few acquisitions [see Fig. 1(b)]. The phase due to the DEM error is simulated using (2) employing typical parameters of the Envisat Advanced SAR (ASAR) sensor. The estimated displacement history after time-series inversion without considering any DEM error correction [see Fig. 1(c)] varies by 9 cm between acquisitions, although the simulated displacement history is zero. The estimated displacement in Fig. 1(c), which is actually the time-series effect of the DEM error, is proportional to the baseline history of the simulated data shown in Fig. 1(b), as we expect from (5).

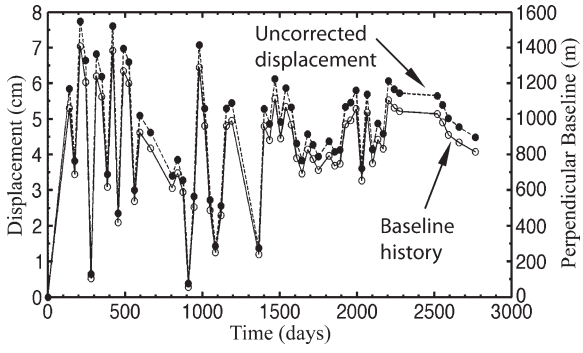

Fig. 3. Baseline history in Fig. 2(b) and uncorrected displacement in Fig. 2(c). The correlation between two histories is due to the effect of the DEM error.

B. DEM Error Correction

We now simulate a more realistic set of interferograms based on the real baseline history of 59 Envisat SAR acquisitions covering Fernandina volcano used in Section V. The network of simulated interferograms (perpendicular baselines less than 400 m and temporal separation less than 900 days) and the perpendicular baseline history are shown in the baseline–time plots in Fig. 2(a) and (b), respectively. The range of the baseline history of the whole data set is around 1400 m. For the interferogram simulation, we consider a DEM error of 20 m and four different displacement histories: 1) zero displacement; 2) constant velocity typical for tectonic processes; 3) exponential temporal displacement; and 4) complex time-variable

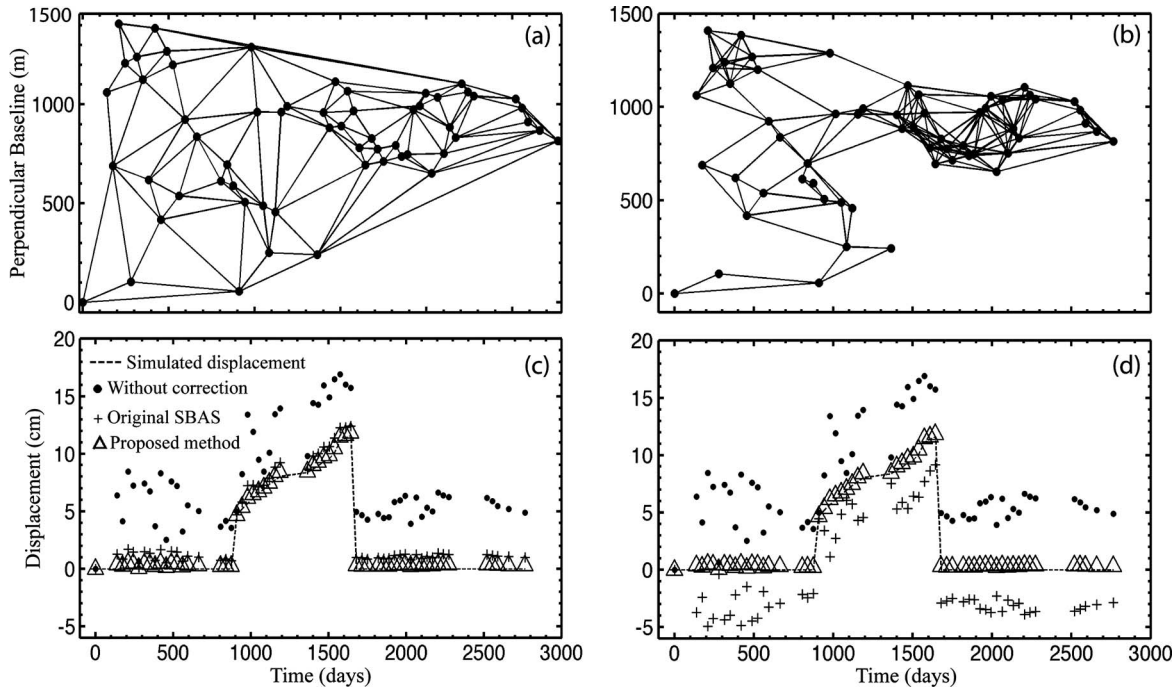

Fig. 4. Effect of interferogram network on DEM error correction (simulated data). (a) Delaunay triangulated network. (b) Network consisting of all interferograms with spatial and temporal baseline thresholds of 300 m and 900 days with incoherent interferograms removed manually. (c) and (d) Same as Fig. 2(f). See Fig. 2(a) for the network with thresholds of 400 m and 900 days (without removing interferograms) and Fig. 2(f) for the corresponding displacement histories. For complex time-variable displacement, the new method is independent of the interferogram network, but the original SBAS method is dependent on the interferogram network.

displacement including rapid uplift and subsidence typical for volcanic processes.

The simulated and estimated displacement time series are shown in Fig. 2(c)–(f). The uncorrected displacements in this figure are the result of time-series inversion of the simulated interferograms using the SB method without DEM error correction. The estimated displacement histories without DEM error correction (filled circles) differ from the simulated ones (dashed lines) in all cases because of the DEM error effect. In the absence of deformation [see Fig. 2(c)], it can be clearly seen that the estimated displacement history without DEM error correction is proportional to the baseline history in Fig. 2(b). Fig. 3 shows this correlation clearly. In the three cases in Fig. 2(c)–(e), the estimated displacement histories after the DEM error correction (triangles) equal the simulated displacement histories. In these cases, the displacement histories are simple and well described by the polynomial deformation model in (6). For the last case [Fig. 2(f)], the estimated displacement history differs from the simulated one by 1 cm (or less) at each epoch. This difference is the result of the inadequate temporal model representation of the surface deformation.

We also compare our new method for DEM error correction with the original SBAS method (plus signs). For the simple cases, the original SBAS method retrieves the simulated displacement history perfectly as does the new method [see Fig. 2(c)–(e)]. For the complex displacement history, the difference for the original SBAS method is more significant than that for the new method [Fig. 2(f)].

To better understand the difference between the new and the original DEM error correction method, we consider different networks of interferograms for the same set of SAR acquisitions. We consider a Delaunay triangulated network [see Fig. 4(a)] and another network with thresholds of 900 days and 300 m for the temporal separation and spatial baseline of the interferograms [see Fig. 4(b)], respectively, in addition to the SB network in Fig. 2(a). The latter is the same network of the Envisat SAR data used in Section V.

For the three cases, the displacement histories estimated using the new method are nearly identical and close to the simulated displacement, whereas the original SBAS method leads to different results [see Figs. 2(f) and 4(c) and (d)]. These differences occur because the original SBAS method estimates the DEM error and parameters of the deformation model in the interferogram domain. When the actual ground displacement cannot be approximated by the deformation model, the DEM error estimation is biased, and different interferogram networks lead to different estimates. In contrast, in our algorithm, which operates in the time domain, the estimation is independent of the network of interferograms.

Another experiment demonstrates how the estimated DEM error depends on the network of interferograms. We test four different networks (Fig. 5). The first network is a sequential network in which interferograms are formed from two consequent acquisitions [Fig. 5(a)]. This network is unrealistic because some interferograms have too-long baseline, but it is useful for this demonstration. The second and third networks are identical to the first except for one additional interferogram, which covers a time period with significant displacement [Fig. 5(c)] and a time period without significant displacement [Fig. 5(e)], respectively. The fourth network is a treelike network commonly used in PS time-series algorithms [Fig. 5(g)].

The estimated displacement histories with DEM error correction using the original SBAS method, with DEM error correction using the new method, and without DEM error correction are shown in the right panels in Fig. 5. In the first

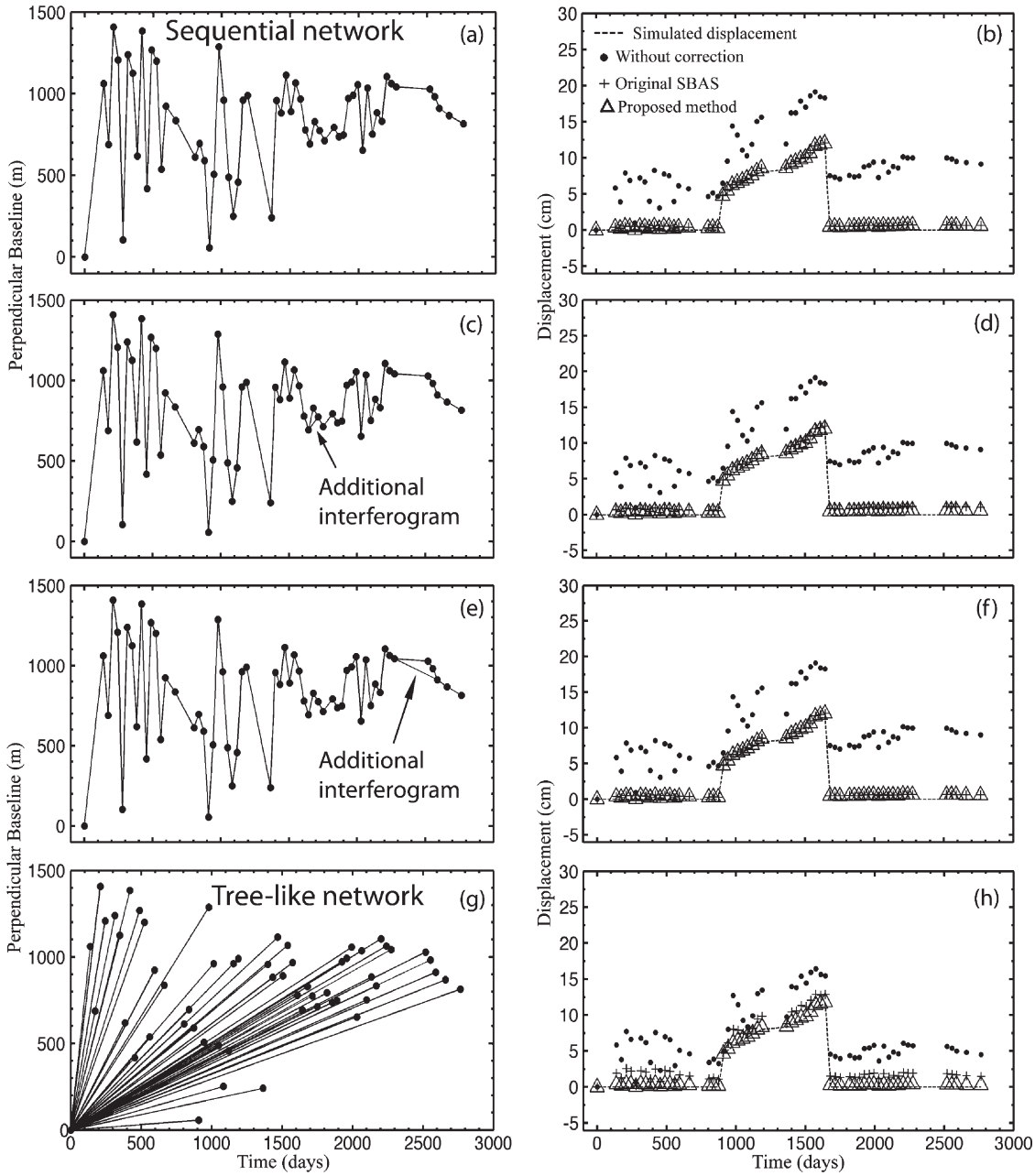

Fig. 5. Simulated data demonstrating the difference between DEM error estimations in the time and interferogram domains. The left panels show different networks of interferograms, and the right panels show the corresponding estimated displacements before and after DEM error correction. DEM error estimation in the interferogram domain depends on the network of interferograms. The estimation in the time domain using the phase velocity history is equivalent to the estimation in the interferogram domain using a sequential network of interferograms.

and third cases, the estimated displacement histories using the original SBAS method and the new method are identical. In the second case, the original SBAS method produces a biased solution. This shows that, in the interferogram domain, one additional interferogram can change the least squares solution for the DEM error if it covers a time period of displacement not described by the assumed deformation model. This also explains the biased estimation of the DEM error using the original SBAS method using the treelike network in Fig. 5(h) and using the SB networks in Figs. 2(f) and 4. To understand why the original SBAS method produces more biased results than the new method, it is instructive to compare the solution in the time domain from the phase velocity history (the new method) with that obtained from the phase history. Fig. 6 shows that the phase velocity gives a less biased solution than the phase history.

This can be explained as follows. The phase history consists at each epoch of values relative to the reference epoch. Thus, at each epoch, it can be considered as a hypothetical interferogram between that epoch and the reference epoch. The entire phase history can then be considered as a treelike network of interferograms. On the other hand, the phase velocity history can be considered as a sequential network of interferograms. In other words, the time-domain estimation of DEM error from the phase history is equivalent to interferogram-domain estimation using a treelike network. Time-domain DEM error estimation from phase velocity history is equivalent to interferogram-domain estimation using a sequential network

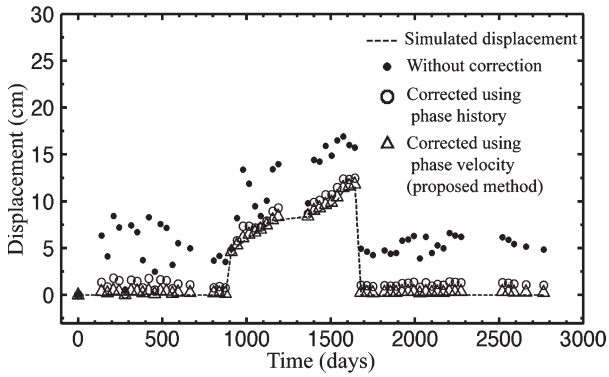

Fig. 6. Comparison of DEM error corrections in the time domain using phase velocity history and phase history. The DEM error is best estimated in the time domain from the phase velocity.

(see Appendix C). As we have shown earlier, the latter is less affected by deficiencies of the assumed deformation model compared to the treelike network. Accordingly, the DEM error is best estimated in the time domain from the phase velocity history rather than from the phase history.

We quantify the effectiveness of the DEM error correction methods using the root-mean-square error (rmse) between the simulated and estimated displacement histories

$$\mathrm{rmse}(\hat{d}) = \left\{ \frac{1}{N} \sum_{i=1}^{N} \left(d(t_i) - \hat{d}(t_i) \right)^2 \right\}^{\frac{1}{2}} \tag{13}$$

where d and $\hat{d}$ are the simulated and estimated displacements, respectively. The rmses for the different displacement histories and interferogram networks in Figs. 2, 4, and 5, with DEM error correction using the new method, with DEM error correction using the original SBAS method, and without DEM error correction, are listed in Table I. The estimated DEM error is also listed. The original simulated DEM error was 20 m in all cases.

The rmse of the estimated displacement history without DEM error correction is 53 mm in all cases. This parameter is zero or nearly zero using both the original SBAS method and the new method for the first two cases with simple displacement histories (linear and exponential). The deviation from zero for the exponential case occurs because this displacement history is not fully approximated by our assumed deformation model. For the cases with complex time-variable displacement history, the new method leads to more accurate results compared to the original SBAS method for most networks. Only for the sequential network and the second modified sequential network (Sequential2), the results are identical for both methods. The table clearly shows that the DEM error estimated with the original SBAS method can depend on the network of interferograms used. In the above analysis, we only have considered connected networks. Any discontinuity in the network would decrease the rank of the matrix B in [5] and leads to additional bias of the estimated displacement history and DEM error.

C. Effect of Atmospheric Delays on DEM Error Estimation

The effect of atmospheric delays on the DEM error estimation is demonstrated in Fig. 7. We use the exponential displacement history in Fig. 2(e). We simulate the atmospheric phase contribution as additive random Gaussian noise. We consider a DEM error of 20 m. Thus, phase histories have contributions from displacement, DEM error, and atmospheric delay. We compare the estimated phase histories before and after DEM error correction (converted into displacements for simplicity; the filled circles and triangles in Fig. 7) with the simulated phase histories (dashed lines). For small atmospheric noise (standard deviation of 7 mm), the simulated phase history is well retrieved [see Fig. 7(a)]. For significant atmospheric noise (standard deviation of 30 mm), the estimated phase history differs from the simulated one [see Fig. 7(b)]. This occurs because strong atmospheric delays cause the noise term $\dot{\psi}_i$ in (8) to be large and result in a biased DEM error estimation. Orbital errors and thermal noise have similar effects as atmospheric noise on DEM error estimation.

D. Effect of Temporal Behavior of Baseline History on DEM Error Estimation

A characteristic of the cases discussed earlier is that the baseline and displacement histories are not correlated, which is favorable for DEM error estimation. Such baseline histories are typical for the Envisat and European Remote-sensing Satellites (ERS-1 and ERS-2). When the displacement and baseline histories are correlated, it is not possible to estimate the DEM error. This can be the case for ALOS PALSAR [15]. Typical ALOS baseline histories are shown in Fig. 8. The baseline history has irregular temporal behavior at the equator [Fig. 8(a)] and sawtooth-type behavior at midlatitudes and high latitudes [period of about two years; Fig. 8(b)].

In the first case, the baseline and displacement histories are unlikely to be correlated, and the DEM error can be estimated. The problems associated with the second case are demonstrated in Fig. 9. We assume zero deformation and a DEM error of 20 m. For a linear baseline history [e.g., SAR acquisitions from 2009 to 2011 from Fig. 8(b)], the simulated displacement history is not retrieved [Fig. 9(a) and (c)]. The estimated displacement histories before and after DEM error correction are both proportional to the baseline history with the slope representing the DEM error. If the linear baseline increase is followed by a discontinuity [Fig. 9(b)], the simulated displacement history is retrieved, indicating that the DEM error can be properly estimated [Fig. 9(d)].

V. Real Data

Fernandina Island is one of the Galapagos Islands located around 1000 km west of Ecuador (see Fig. 10) [18], [19]. This volcanic island is considered as one of the most active volcanoes in the world with at least 15 eruptions during 1950–2010. Two major eruptions occurred in May 2005 and April 2009, and two seismic swarms occurred in December 2006 and August 2007 [20].

We used a data set of 59 Envisat ASAR images from March 11, 2003, to September 7, 2010, acquired along the descending satellite orbit (track 412, frame 3609, beam I2). During the InSAR processing, we estimate the topographic phase using a Shuttle Radar Topography Mission DEM with 90-m pixel size downsampled to 30 m. We took five looks in the azimuth direction to obtain roughly square pixels. The perpendicular baseline history of SAR images and the network of interferograms are shown in the baseline-time plots in Figs. 2(b) and 4(b), respectively (perpendicular baselines less than 300 m,

TABLE I
RMSEs FOR THE ESTIMATED DISPLACEMENT HISTORIES WITH AND WITHOUT DEM ERROR CORRECTION. THE SIMULATED DEM ERROR IS 20 m IN ALL CASES. SB1 IS AN SB NETWORK WITH PERPENDICULAR AND TEMPORAL BASELINE THRESHOLDS OF 400 m AND 900 DAYS; SB2 IS WITH THRESHOLDS OF 300 m AND 900 DAYS AND INCOHERENT INTERFEROGRAMS REMOVED. SEQUENTIAL1 IS A NETWORK WITH EACH INTERFEROGRAM FORMED FROM TWO CONSEQUENT ACQUISITIONS. SEQUENTIAL2 AND SEQUENTIAL3 HAVE TWO ADDITIONAL INTERFEROGRAMS AS SHOWN IN FIG. 5(c) AND (e), RESPECTIVELY

Displacement history	Network	RMSE(mm)			Estimated DEM error (m)		Figure
		Uncorrected	New algorithm	Original SBAS	New algorithm	Original SBAS	
Linear	SB1	53	0	0	20	20	Fig. 2(c) and (d)
Exponential	SB1	53	0.2	0.9	20.07	20.4	Fig. 2(e)
Time-variable	SB1	53	3	43	18.7	36.2	Fig. 2(f)
	Delaunay	53	3	10	18.7	16.2	Fig. 4(c)
	SB2	53	3	31	18.7	31.7	Fig. 4(d)
	Sequential1	53	3	3	18.7	18.7	Fig. 5(b)
	Sequential2	53	3	5	18.7	17.9	Fig. 5(d)
	Sequential3	53	3	3	18.7	18.7	Fig. 5(f)
	Tree-like	53	3	16	18.7	13.9	Fig. 5(h)

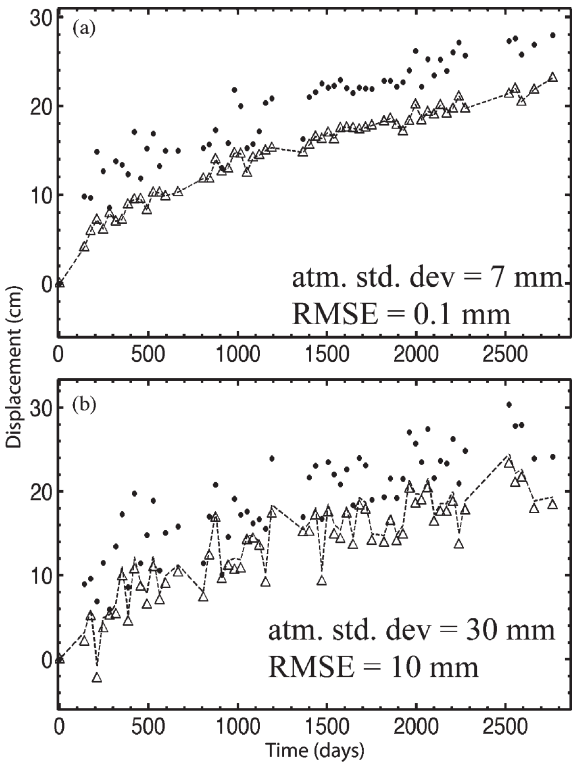

Fig. 7. Effect of atmospheric delay on DEM error correction (simulated data). The filled circles are estimated phase histories (converted to displacements) before DEM error correction, which has contributions from an exponential displacement [same as Fig. 2(e)], 20 m of DEM error, and atmospheric delay with standard deviations of (a) 7 and (b) 30 mm. The (triangles) estimated signals after the DEM error correction have been compared with the (dashed line) simulated displacement plus atmospheric effect, and rmse has been calculated. Significant atmospheric delays can bias the DEM error estimation.

time separation less than 910 days, and manual removal of incoherent interferograms).

Fig. 11(a) shows the estimated displacement histories for a pixel inside the caldera with and without DEM error correction. Without DEM error correction, the estimated displacement history at the beginning of the time period is rough, varying by up to 25 cm between epochs (until 2005). A zoom into this time period [see Fig. 11(b)] shows that the displacement history correlates with the baseline history, indicating a DEM error.

Fig. 11(a) also shows that the uncorrected displacement history does not resolve the subsidence associated with an late 2006 seismic swarm but does resolve the deformation associated with a late-2007 seismic swarm and a 2009 eruption. This is consistent with our expectation about the effect of the DEM error. Over our test area, Envisat had a stable orbit after June 2007 with a range in baseline of less than 400 m [day 1400 in Fig. 2(b)]. Consequently, for this time period, the DEM error has only little effect, and the displacement histories estimated with and without DEM error correction are nearly identical. The shift between them is because of an averaged perpendicular baseline of 900 m with respect to the first acquisition.

VI. CONCLUSION

We have presented the mathematical formulation for the phase due to the DEM error in the InSAR time domain. We have shown that the phase due to the DEM error at each epoch is proportional to the perpendicular baseline between the corresponding SAR acquisition and the temporal reference acquisition. Selecting small-spatial-baseline interferograms typical for the SB time-series approach minimizes the phase due to the DEM error in the interferograms but not in the estimated displacement history. The effect of the DEM error depends on the total range in perpendicular baselines of an interferogram network and not on the baseline of individual interferograms. This explains the need for DEM error correction even if only SB interferograms are used. We have proposed a new algorithm for DEM error correction. In this algorithm, the DEM error correction is estimated in the time domain from the phase velocity history. This is in contrast to the original SBAS method in [5] in which the DEM error is estimated in the interferogram domain from the interferometric phases. For simple ground displacement histories, which are well approximated by the assumed deformation model, the new method is equivalent to the original SBAS method. For complex time-variable displacement histories (typical for volcanic unrest or including earthquakes), the new method yields more accurate estimations of the DEM error and of the displacement history. This occurs because the new method is applied in the time domain and therefore independent of the interferogram network. In contrast, in the original SBAS method, the estimated DEM error may depend on the interferogram network.

APPENDIX A

The baseline of an interferogram, generated from two SAR images acquired at t_A and t_B, is the spatial separation of two

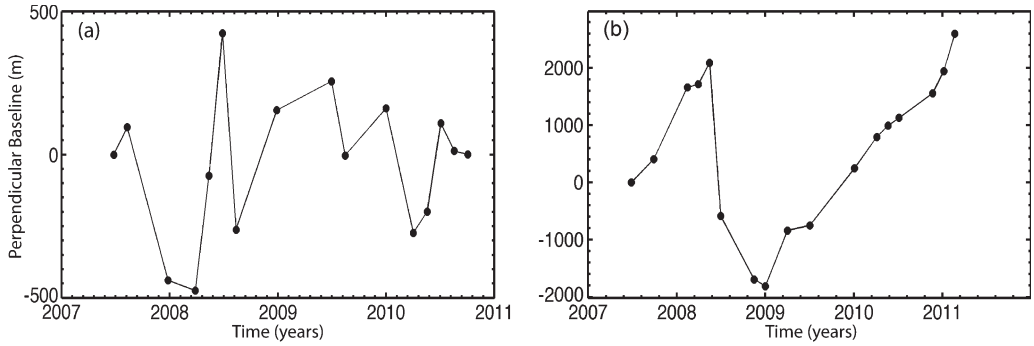

Fig. 8. Baseline history of ALOS PALSAR data sets at different latitudes. (a) 1.5° S covering Tungurahua volcano, Ecuador. (b) 36.5° N covering Cranfield, MS.

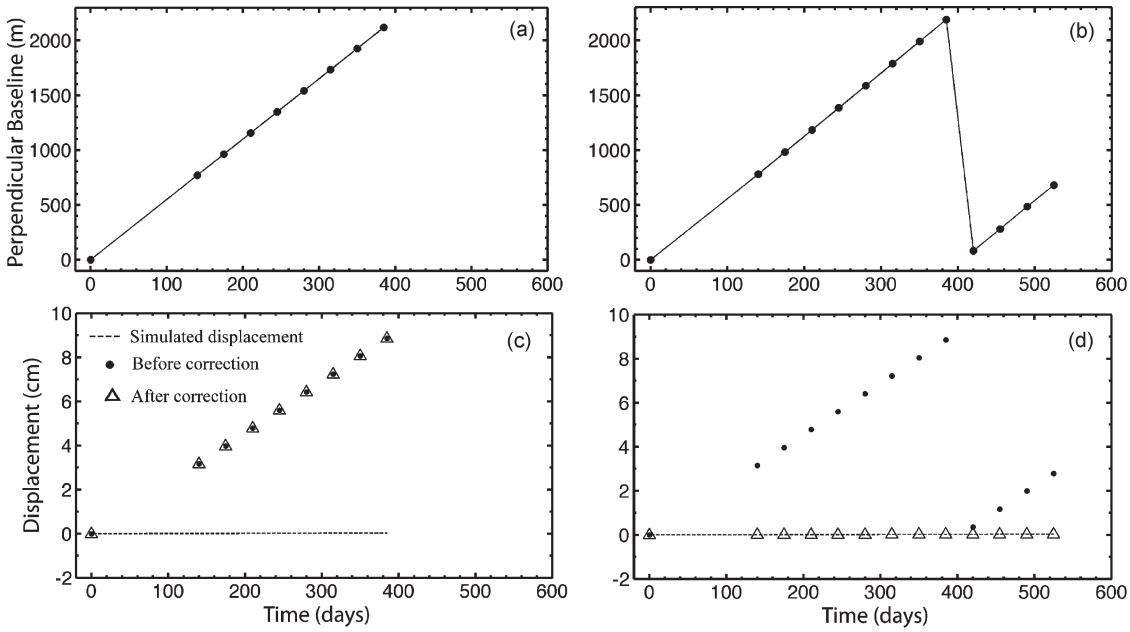

Fig. 9. Effect of the baseline history on DEM error estimation (simulated data). (a) Linear and (b) sawtooth baseline histories. (c) and (d) (Dashed line) Simulated displacement history and estimated displacement histories (circles) before and (triangles) after DEM error correction. For correlating displacement and baseline histories, the DEM error cannot be resolved, resulting in a bias of the estimated displacement history.

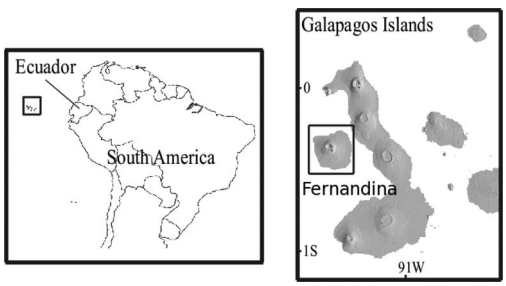

Fig. 10. Location map of Fernandina volcano, Galapagos Islands, Ecuador.

SAR images. Given $\vec{O}(t_i)$ as the vector of the SAR satellite's position at time t_i in an arbitrary coordinate system, the spatial baseline between two SAR acquisitions acquired at times t_A and t_B, i.e., $\vec{B}(t_A, t_B)$, can be expressed as the difference of satellite position vectors at these epochs as follows:

$$\vec{B}(t_A, t_B) = \vec{O}(t_B) - \vec{O}(t_A). \tag{A1}$$

Let us rewrite this equation by simply adding and subtracting the orbital parameters of the reference SAR acquisition (at epoch t_0)

$$\begin{aligned}\vec{B}(t_A, t_B) &= \vec{O}(t_B) - \vec{O}(t_A) + \vec{O}(t_0) - \vec{O}(t_0) \\ &= \left[\vec{O}(t_B) - \vec{O}(t_0)\right] - \left[\vec{O}(t_A) - \vec{O}(t_0)\right] \\ &= \vec{B}(t_B, t_0) - \vec{B}(t_A, t_0)\end{aligned} \tag{A2}$$

wherein $\vec{B}(t_B, t_0)$ and $\vec{B}(t_A, t_0)$ are the spatial baselines between SAR acquisitions acquired at times t_A and t_0 and between t_B and t_0, respectively. By considering t_0 as the reference temporal acquisition, let us simplify (A2) as follows:

$$\vec{B}(t_A, t_B) = \vec{B}(t_B) - \vec{B}(t_A) \tag{A3}$$

where $\vec{B}(t_B)$ and $\vec{B}(t_A)$ by definition are equal to $\vec{B}(t_B, t_0)$ and $\vec{B}(t_A, t_0)$. By considering the parallel and perpendicular

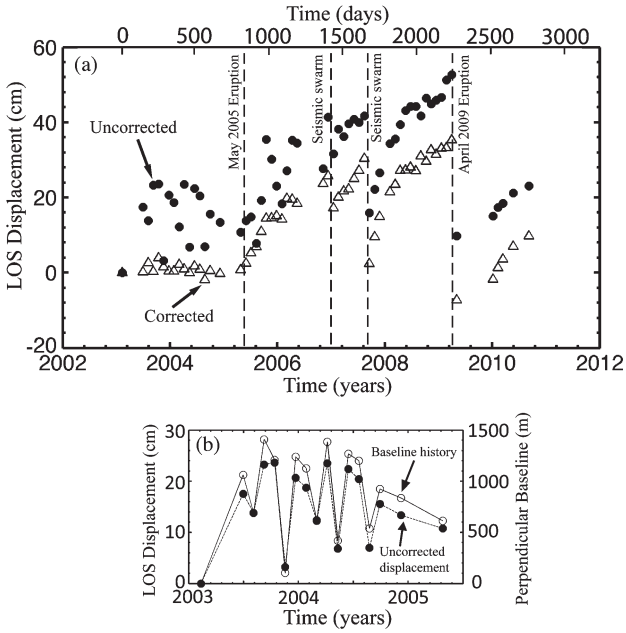

Fig. 11. (a) Estimated displacement histories for a pixel in the center of the Fernandina caldera (circles) before and (triangles) after DEM error correction. (b) (Filled circles and dashed line) Uncorrected displacement history and (open circles and solid line) baseline history for the 2003–mid 2005 time period. This period is characterized by rapid baseline variation [see Fig. 2(b)]. The histories are proportional because of a DEM error. Please note that the total offset due to the 2009 eruption may have been underestimated in C-band ASAR data because of high-phase-gradient problem, since recent results from L-band ALOS PALSAR data show more-than-1-m offset for this eruption [21].

components of the spatial baseline as $\vec{B} = (B_\perp, B_{\rm par})$, the following equation for the perpendicular baseline is valid:

$$B_\perp(t_A, t_B) = B_\perp(t_B) - B_\perp(t_A). \tag{A4}$$

In this paper, $B_\perp(t_i)$ is named baseline history, which, at each epoch t_i, is the perpendicular baseline between SAR images acquired at that epoch and the reference epoch.

APPENDIX B

By considering (7) and the definition of phase velocity as $v_i = (\phi(t_i) - \phi(t_{i-1}))/(t_i - t_{i-1})$, with $i = 1, \ldots, N$, we can obtain (B1), shown at the bottom of the page, for the phase velocity based on the DEM error and parameters of the assumed deformation model.

APPENDIX C

To show that the DEM error estimation in the time domain using phase velocity history is equivalent to that in the interferogram domain with a sequential network, we obtain the design matrix ($[BM, C]$ in [5, eq. (25)]) for DEM error correction of a sequential network of interferograms based on original SBAS (see (C1), shown at the bottom of the page). In this appendix, we use the same symbols as in [5].

The system of equations to estimate the DEM error [5, eq. (25)] takes the following form:

$$[BM, C] \begin{bmatrix} \bar{v} \\ \bar{a} \\ \Delta\bar{a} \\ z^\varepsilon \end{bmatrix} = \begin{bmatrix} \phi_1 - \phi_0 \\ \phi_2 - \phi_1 \\ . \\ . \\ \phi_N - \phi_{N-1} \end{bmatrix}. \tag{C2}$$

The observation vector in the right side of this equation contains interferometric phases identical to the differences in phase history between two consequent epochs. Since we use in the time domain the phase velocity history, let us convert the

$$\begin{aligned} v_i &= \frac{\phi(t_i) - \phi(t_{i-1})}{t_i - t_{i-1}} \\ &= \frac{\bar{v}(t_i - t_0) + \frac{1}{2}\bar{a}(t_i - t_0)^2 + \frac{1}{6}\Delta\bar{a}(t_i - t_0)^3 - \bar{v}(t_{i-1} - t_0) - \frac{1}{2}\bar{a}(t_{i-1} - t_0)^2 - \frac{1}{6}\Delta\bar{a}(t_{i-1} - t_0)^3}{t_i - t_{i-1}} \\ &\quad + \frac{\frac{4\pi}{\lambda}\frac{B_\perp(t_i) - B_\perp(t_{i-1})}{r\sin(\theta)} z^\varepsilon + \psi(t_i) - \psi(t_{i-1})}{t_i - t_{i-1}} \\ &= \bar{v} + \frac{1}{2}\bar{a}(t_i + t_{i-1} - 2t_0) + \frac{(t_i - t_0)^3 - (t_{i-1} - t_0)^3}{6(t_i - t_{i-1})}\Delta\bar{a} + \frac{4\pi}{\lambda}\frac{\dot{B}_{\perp i}}{r\sin(\theta)} z^\varepsilon + \dot{\psi}_i \end{aligned} \tag{B1}$$

$$[BM, C] = \begin{bmatrix} (t_1 - t_0) & \frac{(t_1 - t_0)^2}{2} & \frac{1}{6}(t_1 - t_0)^3 & \frac{4\pi}{\lambda}\frac{B_{\perp(t_0, t_1)}}{r\sin(\theta)} \\ (t_2 - t_1) & \frac{(t_2 - t_1)(t_2 + t_1 - 2t_0)}{2} & \frac{(t_2 - t_0)^3 - (t_1 - t_0)^3}{6} & \frac{4\pi}{\lambda}\frac{B_{\perp(t_1, t_2)}}{r\sin(\theta)} \\ . & . & . & . \\ . & . & . & . \\ (t_N - t_{N-1}) & \frac{(t_N - t_{N-1})(t_N + t_{N-1} - 2t_0)}{2} & \frac{(t_N - t_0)^3 - (t_{N-1} - t_0)^3}{6} & \frac{4\pi}{\lambda}\frac{B_{\perp(t_{N-1}, t_N)}}{r\sin(\theta)} \end{bmatrix} \tag{C1}$$

observation vector to phase velocity by dividing both sides of (C2) by the corresponding time differences. This results in

$$\begin{bmatrix} 1 & \frac{(t_1-t_0)}{2} & \frac{1}{6}(t_1-t_0)^2 & \frac{4\pi}{\lambda}\frac{\dot{B}_{\perp 1}}{r\sin(\theta)} \\ 1 & \frac{(t_2+t_1-2t_0)}{2} & \frac{(t_2-t_0)^3-(t_1-t_0)^3}{6(t_2-t_1)} & \frac{4\pi}{\lambda}\frac{\dot{B}_{\perp 2}}{r\sin(\theta)} \\ . & . & . & . \\ . & . & . & . \\ 1 & \frac{(t_N+t_{N-1}-2t_0)}{2} & \frac{(t_N-t_0)^3-(t_{N-1}-t_0)^3}{6(t_N-t_{N-1})} & \frac{4\pi}{\lambda}\frac{\dot{B}_{\perp N}}{r\sin(\theta)} \end{bmatrix} \times \begin{bmatrix} \bar{v} \\ \bar{a} \\ \Delta\bar{a} \\ z^{\varepsilon} \end{bmatrix} = \begin{bmatrix} v_1 \\ v_2 \\ . \\ . \\ v_N \end{bmatrix}. \quad \text{(C3)}$$

The design matrix in (C3) is identical to (10). This shows that time-domain DEM error estimation from phase velocity history is equivalent to interferogram-domain estimation using a sequential network. In a similar way, it can be shown that time-domain DEM error estimation using phase history is equivalent to interferogram-domain estimation using a treelike network.

ACKNOWLEDGMENT

Envisat SAR data were provided by ESA through a Cat-1 project. The authors thank the anonymous reviewers for their useful comments that improved the quality of this paper.

REFERENCES

[1] D. Massonnet and K. L. Feigl, "Radar interferometry and its application to changes in the Earth's surface," *Rev. Geophys.*, vol. 36, no. 4, pp. 441–500, Nov. 1998.

[2] A. K. Gabriel, R. Goldstein, and H. A. Zebker, "Mapping small elevation changes over large areas: Differential radar interferometry," *J. Geophys. Res, Solid Earth Planets*, vol. 94, no. B7, pp. 9183–9191, 1989.

[3] D. Massonnet, M. Rossi, C. Carmona, F. Ardagna, G. Peltzer, K. Feigl, and T. Rabaute, "The displacement field of the Landers earthquake mapped by radar interferometry," *Nature*, vol. 364, no. 6433, pp. 138–142, Jul. 1993.

[4] F. Amelung, D. L. Galloway, J. W. Bell, H. A. Zebker, and R. J. LaccniaK, "Sensing the ups and downs of Las Vegas: InSAR reveals structural control of land subsidence and aquifer-system deformation," *Geology*, vol. 27, no. 6, pp. 483–486, Jun. 1999.

[5] P. Berardino, G. Fornaro, R. Lanari, and E. Sansosti, "A new algorithm for surface deformation monitoring based on small baseline differential SAR interferograms," *IEEE Trans. Geosci. Remote Sens.*, vol. 40, no. 11, pp. 2375–2383, Nov. 2002.

[6] R. Lanari, F. Casu, M. Manzo, G. Zeni, P. Berardino, M. Manunta, and A. Pepe, "An overview of the small baseline subset algorithm: A DInSAR technique for surface deformation analysis," *Pure Appl. Geophys.*, vol. 164, no. 4, pp. 637–661, Apr. 2007.

[7] R. Lanari, O. Mora, M. Manunta, J. J. Mallorqui, P. Berardino, and E. Sansosti, "A small-baseline approach for investigating deformations on full-resolution differential SAR interferograms," *IEEE Trans. Geosci. Remote Sens.*, vol. 42, no. 7, pp. 1377–1386, Jul. 2004.

[8] T. R. Lauknes, H. A. Zebker, and Y. Larsen, "InSAR deformation time series using an L1-norm small-baseline approach," *IEEE Trans. Geosci. Remote Sens.*, vol. 49, no. 1, pp. 536–546, Jan. 2011.

[9] A. Ferretti, C. Prati, and F. Rocca, "Permanent scatterers in SAR interferometry," *IEEE Trans. Geosci. Remote Sens.*, vol. 39, no. 1, pp. 8–20, Jan. 2001.

[10] A. Hooper, P. Segall, and H. A. Zebker, "Persistent scatterer InSAR for crustal deformation analysis, with application to Volcan Alcedo, Galapagos," *J. Geophys. Res, Biogeosci.*, vol. 112, no. B7, pp. B07407-1–B07407-22, Jul. 2007.

[11] P. Shanker and H. A. Zebker, "Persistent scatterer selection using maximum likelihood estimation," *Geophys. Res. Lett.*, vol. 34, no. 22, pp. L22301-1–L22301-4, Nov. 2007.

[12] A. Ferretti, A. Fumagalli, F. Novali, C. Prati, F. Rocca, and A. Rucci, "A new algorithm for processing interferometric data-stacks: SqueeSAR," *IEEE Trans. Geosci. Remote Sens.*, vol. 49, no. 9, pp. 3460–3470, Sep. 2011.

[13] A. Pepe, P. Berardino, M. Bonano, L. D. Euillades, R. Lanari, and E. Sansoti, "SBAS-based satellite orbit correction for the generation of DInSAR time-series: Application to RADARSAT-1 data," *IEEE Trans. Geosci. Remote Sens.*, vol. 49, no. 12, pp. 5150–5165, Dec. 2011.

[14] H. Fattahi, M. J. Valadan Zoej, M. R. Mobasheri, M. Dehghani, and M. R. Sahebi, "Windowed Fourier transform for noise reduction of SAR interferograms," *IEEE Geosci. Remote Sens. Lett.*, vol. 6, no. 3, pp. 418–422, Jul. 2009.

[15] S. Samsonov, "Topographic correction for ALOS PALSAR interferometry," *IEEE Trans. Geosci. Remote Sens.*, vol. 48, no. 7, pp. 3020–3027, Jul. 2010.

[16] A. Pepe, A. B. Ortiz, P. R. Lundgren, P. A. Rosen, and R. Lanari, "The stripmap–ScanSAR SBAS approach to fill gaps in stripmap deformation time series with ScanSAR data," *IEEE Trans. Geosci. Remote Sens.*, vol. 49, no. 12, pp. 4788–4804, Dec. 2011.

[17] N. Gourmelen, F. Amelung, and R. Lanari, "Interferometric synthetic aperture radar–GPS integration: Interseismic strain accumulation across the Hunter Mountain fault in the eastern California shear zone," *J. Geophys. Res.*, vol. 115, no. 9, pp. B09408-1–B09408-16, Sep. 2010.

[18] S. Jónsson, H. Zebker, P. Cervelli, P. Segall, H. Garbeil, P. Mouginis-Mark, and S. Rowland, "A shallow-dipping dike fed the 1995 flank eruption at Fernandina volcano, Galapagos, observed by satellite radar interferometry," *Geophys. Res. Lett.*, vol. 26, no. 8, pp. 1077–1080, Apr. 1999.

[19] F. Amelung, S. Jónsson, H. Zebker, and P. Segall, "Widespread uplift and trapdoor faulting on Galapagos volcanoes observed with radar interferometry," *Nature*, vol. 407, no. 6807, pp. 993–996, Oct. 2000.

[20] M. Bagnardi and F. Amelung, "Space geodetic evidence for multiple magma reservoirs and subvolcanic lateral intrusions at Fernandina volcano, Galapagos Islands," *J. Geophys. Res.*, vol. 117, no. B10, pp. B10406-1–B10406-19, Oct. 2012.

[21] M. S. Baker, "Investigating the Dynamics of Basaltic Volcano Magmatic Systems With Space Geodesy," Ph.D. dissertation, Univ. of Miami, Miami, FL, 2012.

Heresh Fattahi (S'12) was born in Kurdistan, Iran, in 1982. He received the B.S. degree in civil engineering and geomatics from the University of Isfahan, Isfahan, Iran, in 2004 and the M.S. degree in remote sensing engineering from K. N. Toosi University of Technology, Tehran, Iran, in 2007. He has been working toward the Ph.D. degree in the InSAR Laboratory, Division of Marine Geology and Geophysics, Rosenstiel School of Marine and Atmospheric Science, University of Miami, Miami, FL, since August 2010, where he is currently working on synthetic aperture radar (SAR) interferometry (InSAR) technique and its applications in geophysical studies.

His main research interest is to use multitemporal SAR data to discriminate noise from signals in InSAR displacement time series for studying crustal deformations induced by tectonic and volcanic activities.

Falk Amelung received the M.S. degree in geophysics from the University of Münster, Münster, Germany, in 1992 and the Ph.D. degree from the University of Strasbourg, Strasbourg, France, in 1996.

After several years as a Research Scientist with Stanford University, Stanford, CA, and the University of Hawaii, Honolulu, he joined the University of Miami, Miami, FL, in 2002, where he is currently a Professor of geophysics with the Division of Marine Geology and Geophysics, Rosenstiel School of Marine and Atmospheric Science. His research expertise is the synthetic aperture radar interferometry (InSAR) study of active volcanism, active tectonics, and land subsidence. His particular research goals are the use of InSAR for measuring subtle tectonic deformation and for volcano monitoring.

Dr. Amelung currently chairs the Scientific Advisory Committee of the Geohazard Supersites and Natural Laboratories Initiative of the Group on Earth Observations.